NON-LINEAR COMPLEMENTARY FILTER BASED UPPER LIMB MOTION TRACKING USING WEARABLE SENSORS

Chieh Chien, Jingtao Xia, Oscar Santana, Yan Wang, Greg J. Pottie

University of California, Los Angeles

ABSTRACT

In this paper, we present a method to reconstruct motion trajectories of the upper body using inertial measurement units (IMUs). We combine the use of complementary filters and biomechanical models to reconstruct upper body motions. At rst, we use complementary lters to combine information from low-frequency part of accelerometers and magnetometers, and high-frequency part of gyros to estimate sensor orientations and gyro bias. Then we use the estimated orientations of the upper arm and forearm to calculate trajectories of upper limb movements. Finally, we determine the set of parameters for complementary lters that minimized training errors. Experimental results indicate higher than 90% accuracy using accelerometers, gyros and magnetometers.

Index Terms— Complementary filters, Motion tracking, IMUs

1. INTRODUCTION

IMUs are widely used due to their low cost, lightweight and small size. They are now implemented into numerous fields including aviation, robotics, gaming, sports and others to measure orientations or directions[1, 2, 3, 4]. Some studies also utilized inertial sensing to classify human activities or reconstruct human motions [5, 6, 7, 8, 9, 10].

Generally used IMUs include accelerometers, gyros, magnetometers, GPS and other devices. Due to their physical characteristics and numerical data manipulating procedures, estimation results using these devices suffer from high measurement noise, incorrect scaling and biasing. Therefore, there are many studies discussing how to model measurement errors and drift using various filters and algorithms[11, 12, 13].

Our goal is to estimate the orientations of upper limbs at any given moment to find the motion trajectories of the arm. This will benefit medical-field studies which focus on long-term and detailed movement monitoring. For diseases such as Parkinsons disease or rehabilitation from injuries, doctors and therapists usually need to watch tiny changes of patients' motions for a period of time outside the hospitals. If there exists a system composed of IMUs, which can tell them any instant changes of the motions at patients' home environments, it would greatly benefit doctors' diagnosis and save huge amount of medical resources.

Much research has been conducted to reconstruct trajectories, or to estimate sensor orientations. In [9] kinematic models were combined with unscented Kalman filters to estimate orientations of joints under slow and fast motions. However only simple arm movements were evaluated. In [10], a continuous-wavelet-transform based method was used to integrate accelerometer data analytically to avoid numerical integration drifts, in which subjects only performed motions slowly, and some reconstructed patterns are only recognizable but not accurate.

In this paper, we estimated motion trajectories by combining non-linear complementary filter design, which estimated orientations and gyro bias[3, 14], with biomechanical models of upper limbs, including limb decomposition and human motion limitations. Experiments were conducted covering arm movements, pattern drawing and daily life activities. This method not only applies to upper limb motion reconstruction, but can be also used to estimate orientation of lower limbs with the appropriate kinematic model.

2. ALGORITHMS

2.1. Definitions and Measurement Modeling

In geometry, every rotation matrix $R \in \mathbb{R}^{3\times3}$ belongs to the special orthogonal group SO(3), that is, every rotation matrix satisfies $R^T = R^{-1}$. Also, every orientation can be expressed as a vector $v \in \mathbb{R}^3$ where v contains yaw, pitch and roll angles of the orientation. In this study we define the operator $\vee : \mathbb{R}^3 \to \text{SO(3)}$ such that

$$v_\vee = \begin{pmatrix} 0 & -v_3 & v_2 \\ v_3 & 0 & -v_1 \\ -v_2 & v_1 & 0 \end{pmatrix} \quad v \in \mathbb{R}^3, v_\vee \in \text{SO(3)}$$

We define $\text{vex} : \text{SO(3)} \to \mathbb{R}^3$ being the inverse of $\vee$, thus we have $(\text{vex}(R))_\vee = R, R \in \text{SO(3)}$

We define subscript and superscript A to represent the Earth frame of reference, for which in this paper we use x, y, and z axes to represent north east down (NED) directions.

Financial support provided by the NSF via NetSE Large: Fieldstream: Network Data Services for Exposure Biology Studies in Natural Environments, and the Broadcom Foundation via Medical Technology in Communication

We use B to represent the body frame of reference, and E to represent the estimator frame of reference. For instance, ${}_B v$ represents the orientation v relative to the body frame; ${}^A_B R$ represents the orientation matrix R from Earth frame to the body frame.

Let the noisy data of accelerometers, gyros and magnetometers relative to the body frame be denoted by ${}_B\tilde{a}$, ${}_B\tilde{\omega}$, and ${}_B\tilde{m}$, while the true values are ${}_B a$, ${}_B\omega$, and ${}_B m$. In this paper, we model the relation of collected signals to their true values by

$$
\begin{aligned}
{}_B\tilde{a} &= {}_B a + b_a + n_a \\
{}_B\tilde{\omega} &= {}_B\omega + b_\omega + n_\omega \\
{}_B\tilde{m} &= {}_B m + b_m + n_m
\end{aligned}
$$

where b_a, b_ω, b_m, are the constant bias of the measurement, and n_a, n_ω, n_m are zero-mean additive white Gaussian noise.

2.2. Non-linear Complementary Filter with Bias Estimation

In this section, we describe how to transform sensor orientations ${}^A_E\hat{R}$ from the estimator frame to the Earth frame with noisy measurements. This value should be close to the true orientation from the body frame to the Earth frame, which is ${}^A_B R$.

Ideally, any two nonparallel measurements can be used to calculate the orientation. Thus, we can estimate the orientations of a rigid body given measurements from accelerometers and magnetometers. We call this estimate the static orientation ${}^A_E\hat{R}_s$. It can be acquired using

$$
{}^A_E\hat{R}_s = \underset{R\in \mathrm{SO(3)}}{\arg\min} \left(\| \frac{R \cdot_B \tilde{a}}{\|{}_B\tilde{a}\|} - \frac{{}_A g}{\|{}_A g\|} \|^2 + \| \frac{R \cdot_B \tilde{m}}{\|{}_B\tilde{m}\|} - \frac{{}_A m}{\|{}_A m\|} \|^2 \right)
$$

where $\|\cdot\|$ is the vector norm, ${}_A g$ and ${}_A m$ are gravity and Earth's magnetic field in the Earth frame. Usually a suboptimal solution is presented due to the computational complexity of this problem. Here the static estimated is expressed as

$$
{}^A_E\hat{R}_s = \left[\left(\frac{{}_B\tilde{a}}{\|{}_B\tilde{a}\|} \times \frac{{}_B\tilde{m}}{\|{}_B\tilde{m}\|} \right) \times \frac{{}_B\tilde{a}}{\|{}_B\tilde{a}\|} \quad \frac{{}_B\tilde{a}}{\|{}_B\tilde{a}\|} \times \frac{{}_B\tilde{m}}{\|{}_B\tilde{m}\|} \quad \frac{{}_B\tilde{a}}{\|{}_B\tilde{a}\|} \right]^T
$$

where $\times$ denotes the vector cross product.

This static estimate is accurate if the object moves slowly and the measurement error is small, that is, in low frequency conditions we have ${}^A_E\hat{R}_s \approx {}^A_B R$.

We estimate the dynamic orientations ${}^A_E\hat{R}_d$ from kinematic constraints by solving the following differential equation

$$
\frac{\partial}{\partial t} {}^A_E\hat{R}_d = {}^A_E\hat{R}_d \cdot {}_B\tilde{\omega}_\vee = ({}^A_E\hat{R}_d \cdot {}_B\tilde{\omega})_\vee \cdot {}^A_E\hat{R}_d
$$

Since the high frequency part of the gyro data is accurate, the instantaneous change of the dynamic estimation is close ${}^A_B R$. That is, we have $\frac{\partial}{\partial t} {}^A_E\hat{R}_d \approx \frac{\partial}{\partial t} {}^A_B R$.

The rotation error between frames can be expressed as $\tilde{R} = {}^A_E\hat{R}^T {}^A_B R$. Based on [15, 14], we define the correction term

$$
\sigma = \mathrm{vex}\left(\frac{1}{2}(\tilde{R}^T - \tilde{R}) \right) \in \mathbb{R}^3
$$

In this paper, we use σ to represent error between the estimated orientation and the true orientation. When the estimation is equal to the truth, we have $\tilde{R} = I_3$, and thus $\sigma = \begin{bmatrix} 0 & 0 & 0 \end{bmatrix}^T$. With the above definitions, we then fuse static and dynamic estimates to derive the final estimate of the orientation ${}^A_E\hat{R}$.

From kinematics of a rigid body we know for a rotation matrix R we have

$$
\frac{\partial}{\partial t} R = R\omega_\vee = (R\omega)_\vee R
$$

where ω is the angular velocity. By modifying the last term of the equation and based on [3, 15], we define two types of filters.

Direct complementary filter with bias correction

$$
\begin{aligned}
\frac{\partial}{\partial t} {}^A_E\hat{R}^D &= \left({}^A_E\hat{R}_s({}_B\tilde{\omega} - \hat{b}^D_\omega) + k_p {}^A_E\hat{R}^D \sigma \right)_\vee {}^A_E\hat{R}^D & {}^A_E\hat{R}^D(0) &= {}^A_E\hat{R}_{s0} \quad (1a) \\
\frac{\partial}{\partial t} \hat{b}^D_\omega &= -k_I \sigma, & \hat{b}^D_\omega(0) &= \hat{b}^D_{\omega 0} \quad (1b) \\
\sigma &= \mathrm{vex}\left(\frac{1}{2}(\tilde{R}^T - \tilde{R}) \right) & \tilde{R} &= ({}^A_E\hat{R}^D)^T {}^A_E\hat{R}_s \quad (1c)
\end{aligned}
$$

Passive complementary filter with bias correction

$$
\begin{aligned}
\frac{\partial}{\partial t} {}^A_E\hat{R}^P &= \left({}^A_E\hat{R}^P({}_B\tilde{\omega} - \hat{b}^P_\omega) + k_p {}^A_E\hat{R}^P \sigma \right)_\vee {}^A_E\hat{R}^P & {}^A_E\hat{R}^P(0) &= {}^A_E\hat{R}_{s0} \quad (2a) \\
\frac{\partial}{\partial t} \hat{b}^P_\omega &= -k_I \sigma, & \hat{b}^P_\omega(0) &= \hat{b}^P_{\omega 0} \quad (2b) \\
\sigma &= \mathrm{vex}\left(\frac{1}{2}(\tilde{R}^T - \tilde{R}) \right) & \tilde{R} &= ({}^A_E\hat{R}^P)^T {}^A_E\hat{R}_s \quad (2c)
\end{aligned}
$$

where ${}^A_E\hat{R}^D$ and ${}^A_E\hat{R}^P$ are direct and passive estimates of the orientation from the estimator frame to the Earth frame, $\hat{b}^D_\omega$ and $\hat{b}^P_\omega$ are the estimated bias of gyros, k_p and k_I are positive gains.

In [3] it was shown that the estimates of the orientations ${}^A_E\hat{R}^D$ and ${}^A_E\hat{R}^P$, as well as gyro bias estimations b^D_ω and b^P_ω will converge to the true values ${}^A_B R$ and b_ω respectively, and for almost all initial conditions the trajectory $({}^A_E\hat{R}^D(t), \hat{b}^D_\omega(t))$ and $({}^A_E\hat{R}^D(t), \hat{b}^D_\omega(t))$ converge to the trajectory $({}^A_B R, b_\omega)$. In this paper, we use both methods to estimate the orientations of the sensors.

2.3. Upper Body Motion Decomposition

After finding the orientations of sensors using complementary filters, we then use biomechanical models for the upper limbs

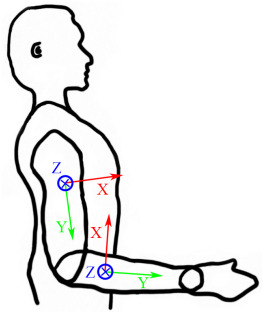

Fig. 1. Position and orientation of sensor placement

to reconstruct human motions. In this model, we assume that the upper limb motions can be decomposed into upper arm and forearm movements. In this paper we put sensors in the middle of these two limbs, and align the y-axis of the sensors with the bone, where the plus direction of the y-axis points outward from the human body. Figure 1 shows positions and orientations of sensor placements. We do not put sensors on the fist and consider the fist as a part that extends from the forearm. Also, we consider the shoulder to be a fixed joint in the space. Therefore, the whole model of the upper limb looks like a double pendulum.

We use a hierarchical model to describe human joints. In this model, parent joints are those closer to the center of the body, while child joints are those connecting to their parents and away from the center. The bones are defined by surrounding parent and child joints, their own orientations, and their lengths. Let the joint m denote a parent joint with its location in the Earth frame ${}_AP_m \in \mathbb{R}^3$. This parent is connected to its child $m+1$ by bone of length l_m with estimated orientation $\hat{R}_{l_m}$. This estimated orientation $\hat{R}_{l_m}$ is the same as that of the sensor attached to the limb. Since the y-axis of the sensor is aligned with the bone, we can define a relative vector ${}_EV = {}_E\begin{bmatrix}0 & l_m & 0\end{bmatrix}^T \in \mathbb{R}^3$ in the estimator frame. This vector represents the direction of the child joint $m+1$ seen by the parent joint m. We can then express the location of the child joint in the estimator frame as

$$ {}_EP_{m+1} = {}_EP_m + \hat{R} \cdot {}_EV \tag{3}$$

This formula describes how we can find positions of child joints given their parents.

In this study, we set the origin at the position of the shoulder joint. Let $\hat{R}_U$ and $\hat{R}_F$ represent the estimated orientations of the upper arm and the forearm respectively. Also, let l_u represent the length of the upper arm, and l_f be the length of the forearm and the fist. Then from equation (3) we can find the positions of the elbow ${}_AP_W$ and the fist ${}_AP_F$ in the Earth frame by

$$ {}_AP_W = \hat{R}_U \begin{bmatrix}0 & l_u & 0\end{bmatrix}^T \tag{4a}$$

$$ {}_AP_F = {}_AP_W + \hat{R}_F \begin{bmatrix}0 & l_f & 0\end{bmatrix}^T \tag{4b}$$

By calculating the ${}_AP_W$ and ${}_AP_F$, we can then estimate upper limb trajectories in NED coordinates.

2.4. Filter Parameter Determination

Since human limbs deform when twisting, they cannot be considered as ideal rigid bodies. Therefore, the above double pendulum model needs to be fixed. We remodel the problem into a supervised training procedure.

At first, we asked subjects to perform some designated motions, and recorded the ground truth. The training motions were designed to be easily followed and were repeated for several times. Later on, we compared the estimated results with the ground truth, and calculated estimation errors. We tuned the parameters (k_p, k_I) in equations (1) and (2) and record estimation errors. Finally, we found out the optimal set of (k_p^*, k_I^*) such that the estimation error is minimized.

In this study, subjects were asked to slowly draw a square of length l on a wall, and they stopped for a while at each vertex. We then rebuilt the training motions using the algorithms of 2.2 and 2.3 with different (k_p, k_I). We compared the reconstructed length to l and found the estimation error. The optimal set (k_p^*, k_I^*) given the minimum error would be used in the testing experiments. In summary, we have

$$ (k_p^*, k_I^*) = \underset{(k_p,k_I)\in(\mathbb{R},\mathbb{R})>0}{\arg\min} \sum_{k=1}^{N-1} \left| \|{}_AP_{F,k+1} - {}_AP_{F,k}\| - l \right| \tag{5}$$

where ${}_AP_{F,j}$ is the position of the fist for the j^{th} vertex of the square.

It turns out that equation (5) is a nonconvex problem, and therefore we exhaustively searched a certain range to find the optimal set. Figure 2 shows an example of the error versus different (k_p, k_I) of the passive complementary filter for one subject. The minimum error of 2.72% happens when $(k_p^*, k_I^*) = (1.3, 0.8)$. For direct complementary filters we have similar results and they are also nonconvex problems.

Once we found the optimal parameters, we then applied them to the testing set, and that completes the training process.

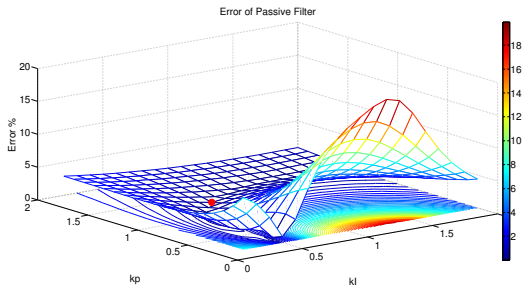

Fig. 2. Error rate with different parameters of passive complementary filters. The red dot marks minimum-error position

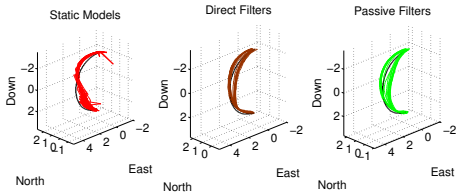

Fig. 3. Vertical arc reconstruction. The ground truth (180°) is shown in black curves.

3. EXPERIMENTAL RESULTS

Several experiments were conducted using a Sparkfun 9 degrees of freedom IMU chip [16] with sampling rate 50Hz. Two sensors were placed in the middle of the upper arm and the forearm as depicted in figure 1. 12 subjects participated in the experiments. In the first experiment subjects were asked to perform 10 rotations around their shoulders from bottom to top for 10 times. Figure 3 shows the 3-dimensional motion reconstruction of the fist movements. Average errors for swing angle estimation are shown in table 1.

In the second experiment subjects drew three shapes on a wall: squares, circles and triangles. The length, height and diameter are 20 inches for squares, triangles and circles respectively. During the experiment, we did not instruct subjects how to draw, that is, how they bend and twist their arms. Each shape took no more than 5 seconds to complete and was repeated for 10 times. Figure 4 (a)-(c) show the reconstructed trajectories with the static model, along with estimates using direct and passive complementary filters. Table 1 shows average errors in estimating lengths for squares and triangles, and radius for circles. From the figure we can see the reconstructed patterns are very close to ground truth, with small errors which are mainly caused from twists of subjects' wrists and deformations of forearms.

Another experiment of pattern drawing was performed, but this time we increased the drawing speed to less than 2 seconds per shape. Figure 4 (d)-(f) shows the reconstructed results. From this figure we can see for the static models that it is hard to recognize the shape since measurement of gravity was severely impeded by fast moves. On the other hand, with the use of complementary filters and biomechnical models the drawn patterns are still clearly recognizable.

The third experiment was conducted to simulate reaching for and grasping books. In this experiment we portioned a 20' by 20' square hanging on a wall into a 3×3 array. Then we

Table 1. Percentage of errors for experiments

Experiment	Direct	Passive	Integration
Vertical arc	9.46	4.68	39.48
Square	6.14	5.04	33.39
Triangle	6.43	6.00	33.54
Circle	4.52	4.23	37.31
Book taking	13.01	12.05	38.86

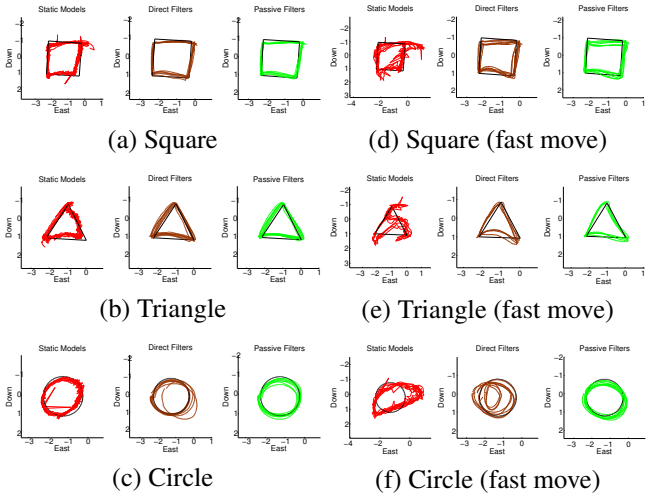

(a) Square (d) Square (fast move)

(b) Triangle (e) Triangle (fast move)

(c) Circle (f) Circle (fast move)

Fig. 4. Reconstruction of pattern drawing, ground truths are shown in black curves

tapped each points 10 times to simulate patients taking books off of a shelf. Figure 5 shows the reconstructed results. The average errors in distances are shown in table 1.

In summary, we had 9.46% and 4.68% error in the arc movement experiment using direct and passive filters, and less than 7% error in the pattern plot experiment. In the book reaching experiment, we had 12% error, compared to 38% error using numerical integration. Compared to prior work [9, 10] the proposed method can track more complex and rapid arm movements. From the figures we can see that the static estimations suffered from sensor noise, deformation of limbs, and external forces that made measurement of gravity inaccurate. On the other side, from table 1 we can see error accumulates using only from integration of gyro data. As a result, the use of complementary filters with a biomechanical model enables us to greatly reduce noise caused by sensors, and eliminate drifts due to numerical integration.

4. CONCLUSION

This paper presents a new algorithm to estimate upper limb motion trajectories using accelerometer, gyro, and magnetometer measurements. This algorithm combines non-linear direct and passive complementary filters and biomechanical models to estimate upper limb trajectories. The estimator also finds the optimal set of parameters for complementary filters to minimize errors caused by noise and limb deformations.

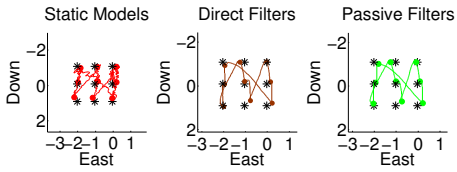

Fig. 5. Reconstruction of book reaching. The ground truth is shown in black stars.

5. REFERENCES

[1] S. Bertrand, T. Hamel, H. Piet-Lahanier, and R. Mahony, "Attitude tracking of rigid bodies on the special orthogonal group with bounded partial state feedback," in *Joint 48th IEEE Conference on Decision and Control and 28th Chinese Control Conference*, pp. 2972–2977, December 2009.

[2] S. P. Tseng, W.-L. Li, C.-Y. Sheng, J.-W. Hsu, and C.-S. Chen, "Motion and attitude estimation using inertial measurements with complementary filter," in *Proceedings of 2011 8th Asian Control Conference (ASCC)*, pp. 863–868, May 2011.

[3] R. Mahony, T. Hamel, and J.-M. Pimlin, "Non-linear complementary filters on the special orthogonal group," *IEEE Transactions on Automatic Control*, vol. 53, pp. 1203–1217, May 2008.

[4] D. Roetenberg, *Inertial and Magnetic Sensing of Human Motion*. PhD thesis, Universiteit Twente, 2006.

[5] C. Chien and G. J. Pottie, "A universal hybrid decision tree classifier design for human activity classification," in *Engineering in Medicine and Biology Society (EMBC), 2012 Annual International Conference of the IEEE*, August 2012.

[6] N. H. C. Ascher Friedman, , C. Chien, and G. J. Pottie, "Estimation of accelerometer orientation for activity recognition," in *Engineering in Medicine and Biology Society (EMBC), 2012 Annual International Conference of the IEEE*, August 2012.

[7] B. Fish, A. Khan, N. H. Chehade, C. Chien, and G. J. Pottie, "Feature selection based on mutual information for human activity recognition," in *IEEE International Conference on Acoustics, Speech, and Signal Processing*, March 2012.

[8] Y. Wang, X. Xu, M. Batalin, and W. Kaiser, "Detection of upper limb activities using multimode sensor fusion," in *Biomedical Circuits and Systems Conference (BioCAS), 2011 IEEE*, November 2011.

[9] M. El-Gohary, L. Holmstrom, J. Huisinga, E. King, J. McNames, and F. Horak, "Upper limb joint angle tracking with inertial sensors," in *33rd Annual International Conference of the IEEE EMBS*, 2011.

[10] S. Suvorova, T. Vaithianathan, and T. Caelli, "Action trajectory reconstruction from inertial sensor," in *The 11th International Conference on Information Science, Signal Processing and their applications*, July 2012.

[11] S. Sukkarieh, E. M. Nebot, and H. F. Durrant-Whyte, "A high integrity imu/gps navigation loop for autonomous land vehicle applications," *IEEE Transactions on Robotics and Automation*, vol. 15, pp. 572–578, June 1999.

[12] S. I. Roumeliotis, G. S. Sukhatme, and G. A. Bekey, "Circumventing dynamic modeling: Evaluation of the error-state kalman filter applied to mobile robot localization," in *International Conference on Robotics and Automation*, pp. 1656–1663, May 1999.

[13] N. El-Sheimy, H. Hou, and X. Niu, "Analysis and modeling of inertial sensors using allan variance," *IEEE Transactions on Instrumentation and Measurement*, vol. 57, pp. 140–149, January 2008.

[14] R. Mahony and T. Hamel, "Attitude estimation on SO(3) based on direct inertial measurements," in *International Conference on Robotics and Automation, ICRA2006*, 2006.

[15] R. Mahony, T. Hamel, and J.-M. Pimlin, "Complementary filter design on the special orthogonal group SO(3)," in *44th IEEE Conference on Decision and Control, and the European Control Conference 2005*, pp. 1477–1484, December 2005.

[16] Sparkfun Electronics, "9 degrees of freedom - razor imu."